AD-A053 286 DCW INDUSTRIES INC STUDIO CITY CA F/G 20/4
RESEARCH ON THE POST-CRITICAL STAGES OF TRANSITION.(U)
JAN 78 D C WILCOX N00014-77-C-0259
UNCLASSIFIED DCW-R-18-01 ONR-CR-289-020-1F NL

1 OF 1
AD
A053286

END
DATE
FILMED
6-78
DDC

(12)

DCW INDUSTRIES

4367 TROOST AVENUE, STUDIO CITY, CALIFORNIA 91604

Change of Address

Organizations receiving reports on the initial distribution list should confirm correct address. This list is located at the end of the report. Any change of address or distribution should be conveyed to the Office of Naval Research, Code 211, Arlington, VA 22217.

Disposition

When this report is no longer needed, it may be transmitted to other organizations. Do not return it to the originator or the monitoring office.

Disclaimer

The findings and conclusions contained in this report are not to be construed as an official Department of Defense or Military Department position unless so designated by other official documents.

Reproduction

(12)

REPORT ONR-CR289-020-1F

RESEARCH ON THE POST-CRITICAL STAGES OF TRANSITION

David C. Wilcox

DCW INDUSTRIES, INC.
Studio City
California
91604

CONTRACT N00014-77-C-0259
ONR TASK 289-020

January 1978

FINAL TECHNICAL REPORT

PREPARED FOR THE

OFFICE OF NAVAL RESEARCH ● 800 N. QUINCY ST. ● ARLINGTON ● VA ● 22217

(9) Final technical rept. 1 Mar 77-31 Jan 78

UNCLASSIFIED

SECURITY CLASSIFICATION OF THIS PAGE (When Data Entered)

REPORT DOCUMENTATION PAGE

READ INSTRUCTIONS BEFORE COMPLETING FORM

1. REPORT NUMBER: ONR-CR289-020-1F
2. GOVT ACCESSION NO.
3. RECIPIENT'S CATALOG NUMBER

4. TITLE (and Subtitle): (6) RESEARCH ON THE POST-CRITICAL STAGES OF TRANSITION.

5. TYPE OF REPORT & PERIOD COVERED: FINAL REPORT 1 MARCH 1977 - 31 JAN 1978

6. PERFORMING ORG. REPORT NUMBER: (14) DCW-R-18-01

7. AUTHOR(s): (10) DAVID C. WILCOX

8. CONTRACT OR GRANT NUMBER(s): (15) N00014-77-C-0259 new

9. PERFORMING ORGANIZATION NAME AND ADDRESS:
DCW INDUSTRIES, INC.
4367 Troost Avenue
Studio City, California 91604

10. PROGRAM ELEMENT, PROJECT, TASK AREA & WORK UNIT NUMBERS:
61153N-31
RR031-01-81
NR289-020

11. CONTROLLING OFFICE NAME AND ADDRESS:
OFFICE OF NAVAL RESEARCH, VEHICLE TECH. PROGRAM
Code 211, 800 North Quincy Street
Arlington, Virginia 22217

12. REPORT DATE: (11) JAN 1978

13. NUMBER OF PAGES: 37 (12) 42p.

14. MONITORING AGENCY NAME & ADDRESS(if different from Controlling Office):
(18) ONR
(19) CR289-020-1F

15. SECURITY CLASS. (of this report): UNCLASSIFIED

15a. DECLASSIFICATION/DOWNGRADING SCHEDULE

16. DISTRIBUTION STATEMENT (of this Report):

Approved for Public Release, Distribution Unlimited.

(16) RR03101 (17) RR031081

17. DISTRIBUTION STATEMENT (of the abstract entered in Block 20, if different from Report)

18. SUPPLEMENTARY NOTES

19. KEY WORDS (Continue on reverse side if necessary and identify by block number)

(e to the 4th power) lambda

TRANSITION, TURBULENCE MODELING, LINEAR STABILITY THEORY

20. ABSTRACT (Continue on reverse side if necessary and identify by block number)

Linear-stability computations for the Blasius boundary layer have been performed in order to evaluate closure coefficients appearing in the Wilcox-Traci two-equation model of turbulence. The computations show that the key closure coefficient affecting the model's ability to accurately predict transition, λ, is strongly frequency dependent until a given boundary-layer disturbance has been amplified to about e^4 times its initial value. Beyond this point, λ approaches an asymptotic profile which is independent of frequency, provided the boundary layer is unstable. Although further investigation is needed, results show → next page

DD FORM 1 JAN 73 1473 EDITION OF 1 NOV 65 IS OBSOLETE

UNCLASSIFIED

SECURITY CLASSIFICATION OF THIS PAGE (When Data Entered)

S/N 393352 JOB

promise that a sound, physically-founded synthesis of linear-stability and turbulence-model methods is possible.

CONTENTS

LIST OF ILLUSTRATIONS

1. INTRODUCTION

Advanced design of aerodynamic and hydrodynamic vehicles often depends critically upon an understanding of transition sensitivity to many phenomena. Nosetips on ballistic reentry vehicles, for example, must be designed to withstand transition destabilizing effects of surface roughness, ablation, surface cooling (in the presence of roughness), and entropy gradient. As a second example, current advanced hydrodynamic vehicle design procedures make advantageous use of the strong stabilizing effects of favorable pressure gradient and surface heating to generate laminar-flow vehicles. Linear stability theory is the most popular theoretical tool for guiding design of many vehicles for which transition location influences the design configuration. While linear stability theory has proven irrelevant for reentry vehicle nosetips (because of the occurrence of roughness-induced transition bypass), a great deal of success with stability theory has been enjoyed for hydrodynamic vehicles, most notably by Wazzan and Smith.[1]

For transition triggered by small amplitude disturbances, linear stability theory provides a nearly exact solution to the Navier-Stokes equations. There is little doubt that stability theory's Tollmien-Schlichting waves exist and play an important role in the initial stages of transition. Because the end state of the transition process is a (highly nonlinear) turbulent flow, linear stability theory breaks down at some point between that of the initiation of Tollmien-Schlichting waves and the transition point (defined, for example, as the point where skin friction achieves a minimum). In other words, linear stability theory is inapplicable in the post-critical stages of transition and therefore has no natural way of specifying the actual transition point.

Undaunted by this limitation on stability theory's applicability, Smith[2] and van Ingen[3] simultaneously (with no knowledge of the other's activities) devised the well-known e^9 method. As is so often the case with clever approximations, the e^9 method has yielded accurate predictions for flows well beyond the original data base. However, the record of success has been blemished somewhat by inaccurate predictions including, surprisingly, applications such as transition sensitivity to freestream turbulence with varying spectral content.

Presumably, either a nonlinear stability theory or an exact Navier-Stokes solution method is needed to rigorously bridge the gap between the initiation of Tollmien-Schlichting waves and the transition point. Because neither of these two approaches has been developed to the point of being practicable for engineering design, the designer must depend upon existing correlations and/or approximate methods such as the e^9 method.

Recently, a new approximate transition-prediction method has been devised which shows great promise for engineering design, viz, the turbulence-model transition-prediction method.[4-6] The method is based on the conventional long-time averaged equations of motion. Nonlinear correlation terms such as the Reynolds stress are approximated in a manner similar to that used in standard closure schemes for turbulent flow modeling. As will be explained in greater detail in Section 2, turbulence-model equations on the one hand are expected to apply in the latter stages of transition. On the other hand, the time-averaging process removes explicit appearance of Tollmien-Schlichting waves. Consequently, the turbulence-model transition-prediction method is reasonly well founded only near the end of transition.

As with the linear-stability/e^9 method, turbulence-model equations have provided accurate transition predictions well beyond the original data base. In fact, the equations formulated by Wilcox and Chambers[7-9] have yielded accurate results for virtually all of the applications made to date. However, some of this success has been achieved with an adjustable parameter, viz, the freestream turbulence level. Additionally, the method has no natural way of representing spectral effects.

In summary, because correlations generally are limited to a restricted data base, linear-stability/e^9 and turbulence-model methods are the only two comprehensive transition theories which are of practical utility for the aerodynamic/hydrodynamic vehicle designer. The former is theoretically sound only during the initial stages of transition while the latter is well founded only near the end of transition. Hence we reasonably may speculate that a synthesis of these two methods will yield a transition-prediction theory which is fundamentally more sound than either theory standing alone.

The primary objective of this project has been to synthesize linear-stability theory and the turbulence-model transition-prediction method. In so doing, the most immediate result of the proposed research, if successful, would be development of a physically sound alternative to the empirical Smith-van Ingen e^9 procedure. Aside from the advantage of having a more fundamental method for simulating the post-critical stages of transition, the proposed synthesis would obviate the costly eigen-solutions needed to compute amplification ratios beyond the critical Reynolds number. Rather, a straightforward boundary-layer marching computation would be all that is needed in solving the turbulence/transition model equations from the critical Reynolds number up to the transition Reynolds number.

As will be shown in the following sections, an important first step has been taken toward accomplishing the proposed synthesis. Results for the Blasius boundary layer show that the most important (in the context of transitional boundary layers) closure coefficient appearing in the turbulence-model equations approaches a universal limiting value for amplification ratios in excess of about e^4.

2. ANALYSIS

This section first reviews the turbulence-model equations which form the basis of the study. Then, the key closure coefficient controlling transition-prediction accuracy, λ, is cast in terms of linear-stability variables. Finally, the coefficient λ is computed for the Blasius boundary layer over the entire stability spectrum and is found to approach a universal limiting form for amplification ratios in excess of e^4.

2.1 REVIEW OF THE TURBULENCE-MODEL EQUATIONS

2.1.1 The Model Equations

For arbitrary incompressible flows, the model equations are[10,11]

Mass Conservation

$$\frac{\partial u_j}{\partial x_j} = 0 \tag{1}$$

Momentum Conservation

$$\rho u_j \frac{\partial u_i}{\partial x_j} = - \frac{\partial p}{\partial x_i} + \frac{\partial \tau_{ij}}{\partial x_j} \tag{2}$$

Energy Conservation

$$\rho u_j \frac{\partial h}{\partial x_j} = u_i \frac{\partial p}{\partial x_i} - \frac{\partial q_i}{\partial x_i} \tag{3}$$

Turbulent Mixing Energy

$$\rho u_j \frac{\partial e}{\partial x_j} = \left[\alpha^* \sqrt{2S_{ij}^2} - \beta^* \omega\right] \rho e + \frac{\partial}{\partial x_j}\left[(\mu + \sigma^* \rho \varepsilon) \frac{\partial e}{\partial x_j}\right] \tag{4}$$

Turbulent Dissipation Rate

$$\rho u_j \frac{\partial \omega^2}{\partial x_j} = \left\{\alpha \sqrt{2S_{ij}^2} - \left[\beta + 2\sigma\left(\frac{\partial \ell}{\partial x_k}\right)^2\right]\omega\right\} \rho \omega^2 + \frac{\partial}{\partial x_j}\left[(\mu + \sigma \rho \varepsilon) \frac{\partial \omega^2}{\partial x_j}\right] \tag{5}$$

where x_j is position vector. Time-averaged (mean) velocity is denoted by u_j while h, p, ρ and μ are mean enthalpy, pressure, density and molecular viscosity; τ_{ij} and q_i are the shear stress tensor and heat-flux vector. The quantity $S_{ij} = 1/2\ (\partial u_i/\partial x_j + \partial u_j/\partial x_i)$ is the mean strain-rate tensor. The turbulent mixing energy, e, and the turbulent dissipation rate, ω, are needed to define the eddy diffusivity, ε, which is given by the following equation:

$$\varepsilon = e/\omega \tag{6}$$

In order to close this system of equations, the stress tensor and heat flux vectors must be specified. In the Wilcox-Traci turbulence model the stress tensor is assumed to have its principal axes alligned with those of the mean strain-rate tensor so that we write

$$\tau_{ij} = 2(\mu + \rho\varepsilon)\ S_{ij} - \frac{2}{3}\rho e\ \delta_{ij} \tag{7}$$

Also, appealing to the classical analogy between heat and momentum transfer, we write the heat flux vector as

$$q_i = -\left(\frac{\mu}{Pr_L} + \frac{\rho\varepsilon}{Pr_T}\right)\frac{\partial h}{\partial x_i} \tag{8}$$

whre Pr_L and Pr_T are laminar and turbulent Prandtl numbers. The quantity ℓ is the turbulent length scale defined as

$$\ell = e^{\frac{1}{2}}/\omega \tag{9}$$

The turbulent Prandtl number, Pr_T, and the closure coefficients $\alpha,\alpha^*,\beta,\beta^*,\sigma,\sigma^*$ appearing in Equations (4) and (5) are

$$\left.\begin{aligned} \beta &= \frac{3}{20} & \beta^* &= \frac{9}{100} \\ \sigma &= \frac{1}{2} & \sigma^* &= \frac{1}{2} \\ Pr_T &= \frac{8}{9} \\ \alpha &= \frac{1}{3}[1 - (1-\lambda)\exp(-Re_T/2)] \\ \alpha^* &= \frac{3}{10}[1 - (1-\lambda)\exp(-2Re_T)] \end{aligned}\right\} \tag{10}$$

where Re_T is the turbulent Reynolds number defined by

$$Re_T = \rho e^{\frac{1}{2}}\ell/\mu \tag{11}$$

As will be discussed in the next subsection, transition predictions are most sensitive to the closure coefficient λ appearing in the last two of Equations (10). Detailed study of the viscous sublayer of a turbulent boundary layer[7,10] indicates that accurate sublayer properties can be simulated with (see Figure 1)

$$\lambda = \frac{1}{11} \tag{12}$$

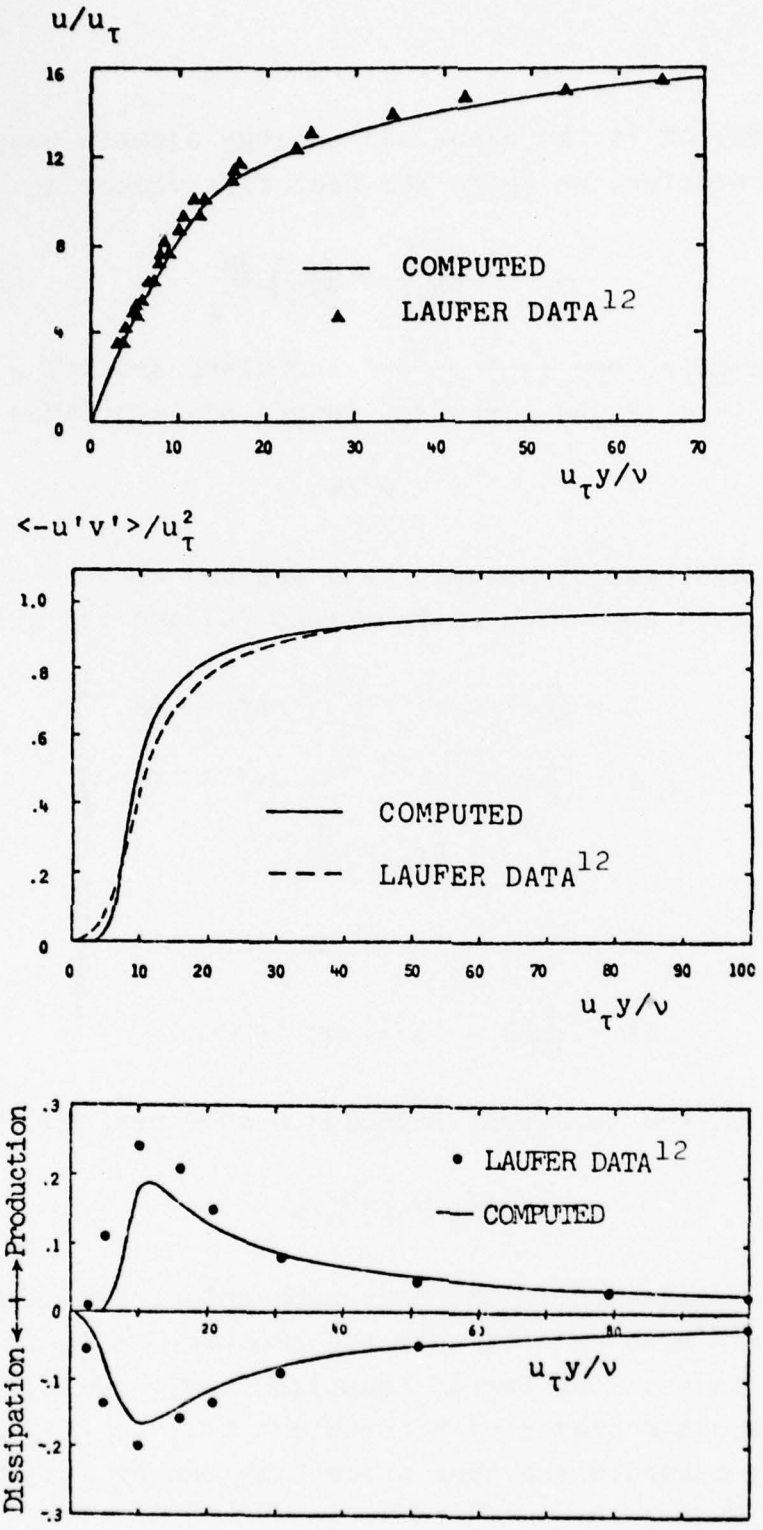

Figure 1. Comparison of computed and measured sublayer properties for a perfectly smooth wall.

Using Equations (1) through (12) (in some cases, similar versions of these equations), a wide range of compressible and incompressible turbulent flows have been computed, including complicating effects such as boundary-layer separation,[13,14] streamline curvature,[15] surface roughness[10] and mass injection.[10] With no additional modifications, the model accurately simulates many aspects of incompressible flat-plate boundary layer (FPBL) transition.[10,11] Hence, at least for the relatively simple FPBL, this model for fully developed turbulent flows provides an accurate description of mean flow properties during transition. And this, despite the fact that the long-time averaging process leading to Equations (1) through (5) masks the presence of any wave-like instability!

Before proceeding to further discussion of why the model does as well as it does and of the value of λ for more complicated flows, it is instructive to present the physical definitions of the turbulence parameters e and ω and appropriate surface boundary conditions for each.

As argued by Wilcox and Chambers,[7,15] the turbulent mixing energy is proportional to the kinetic energy attending the fluctuation of fluid particles normal to the plane of shear. Letting v' denote the fluctuating velocity component normal to the shear plane (under the boundary-layer approximations, shear planes are parallel to the x-z plane), the turbulent mixing energy is given by

$$e = \frac{9}{4} \langle v'^2 \rangle \qquad (13)$$

The physical meaning of ω has also been discussed by Wilcox and Chambers.[7,15] For incompressible boundary layers, comparison of the limiting forms of the model equations and the exact Reynolds stress equation very close to a solid boundary

shows that ω is the rate at which e is dissipated into heat, mean kinetic energy and other fluctuation modes; a suitable definition of ω is

$$\omega = \frac{3\nu}{\beta^*} \frac{\langle (\partial v'/\partial y)^2 \rangle}{\langle v'^2 \rangle} \tag{14}$$

Using the definitions given in Equations (13) and (14), boundary conditions appropriate for smooth and rough surfaces have been devised by Wilcox and Chambers[7] and by Wilcox and Traci.[10] Letting k denote (peak-to-valley) roughness height, detailed study of the viscous sublayer shows that (in the limit of small roughnesses):

$$e = 0 \qquad \text{at} \quad y = 0 \tag{15}$$

$$\omega \to \begin{cases} \dfrac{20}{\beta} \dfrac{\nu_w}{y^2} & \text{, smooth surfaces} \\ 4320 \dfrac{\nu_w}{k^2} & \text{, rough surfaces} \end{cases} \qquad \text{as} \quad y \to 0 \tag{16}$$

2.1.2 Fundamental Considerations

The only feature of transitional boundary layers which has been explicitly introduced into the model is the following. Concurrent with our analysis of the viscous sublayer, the value of λ has been established by demanding that the linear-stability minimum-critical Reynolds number, Re_{x_c}, for the Blasius boundary layer match the corresponding model-equation neutral-stability Reynolds number, $Re_{\tilde{x}}$. The latter is defined as the Reynolds number based on the plate length beyond which turbulent energy production, $\alpha^* |\partial u/\partial y| \rho e$, exceeds turbulent energy dissipation, $\beta^* \rho \omega e$. Using the Blasius profile and noting that $\omega \doteq 20\nu/\beta y^2$ [see Equation (16)], the neutral stability Reynolds number is

$$Re_{\tilde{x}} \doteq \frac{750}{\lambda^2} \qquad (17)$$

Demanding that $Re_{x_c} = Re_{\tilde{x}}$ yields the value of λ given in Equation (12).

The model equations reasonably can be expected to apply to transitional flows which are insensitive to spectral effects. That is, the various constants in the model equations are essentially correlation coefficients which have been integrated over the turbulent spectrum. Hence, if the stability diagram shows that a wide range of wave numbers, $\hat{\alpha}$, undergo amplification, the spectrum will more closely resemble a fully-turbulent spectrum than if only a small range of wave numbers are unstable. For example, the stability diagram for a boundary layer subjected to a pressure gradient is shown in Figure 2. For adverse pressure gradient, a finite range of wave numbers are unstable at all Reynolds numbers in excess of Re_{x_c} (note that δ^* is displacement thickness). On the basis of the discussion above, the model would be expected to accurately predict the destabilizing effect of adverse pressure gradient. In contrast, the stability diagram becomes thinner with increasing favorable pressure gradient so that spectral effects become increasingly important, particularly for small freestream turbulence intensity, T', which yields transition at large values of Re_{δ^*}; the model hence would be expected to fare poorly for transitional boundary layers with favorable gradients (and small freestream disturbances). The model behaves just as the above discussion indicates. Excellent agreement between theory and experiment is obtained for adverse gradients while, for low freestream turbulence intensities, the model fails to predict the strong stabilizing effect of favorable gradients.

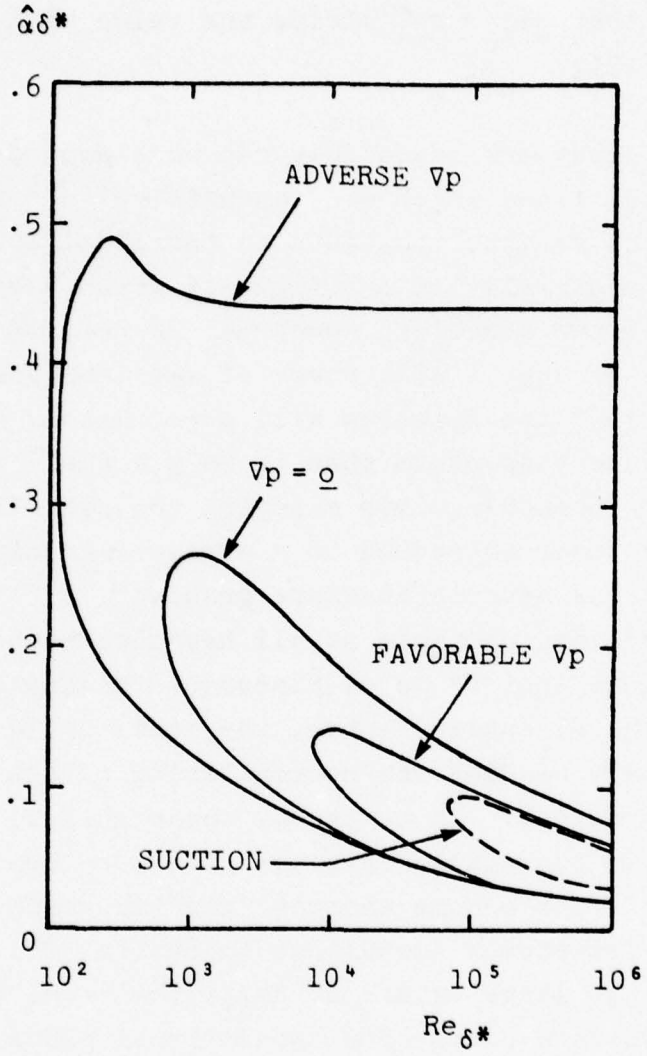

Figure 2. Neutral stability curves for laminar boundary layers with pressure gradient and suction.

To remove this deficiency, Wilcox[11] has extended the requirement

$$Re_{\tilde{x}} = Re_{x_c} \tag{18}$$

to include favorable pressure gradients, suction and surface heating effects. For small freestream turbulence intensity, Equation (12) is replaced by

$$\lambda = \frac{1}{11}\left(\frac{\mu_w}{\mu_e}\right)^{5/2} f(\Lambda) \tag{19}$$

where Λ is given by

$$\Lambda = -\frac{\rho_e}{\rho_w}\frac{\theta^2}{U_e}\left(\frac{\partial^2 u}{\partial y^2}\right)_w \tag{20}$$

and the quantity θ is momentum thickness. The function $f(\Lambda)$ has been determined by invoking Equation (18). Figure 3 presents results based on linear-stability predictions for the Pohlhausen profiles and for the asymptotic suction profile;[16] a good fit to the data indicates the variation of the function $f(\Lambda)$ with Λ is hence

$$f(\Lambda) \doteq \frac{1}{88} + \frac{87}{88}\exp\left[-40\Lambda\, H(\Lambda)\right] \tag{21}$$

where $H(\Lambda)$ is the Heaviside stepfunction.

In essence, Equations (19)-(21) represent a correlation of linear-stability-predicted minimum-critical Reynolds numbers. We have thus implicitly built in some of the wave-instability phenomena which were lost through the long-time averaging procedure. Two key points must be amplified regarding this last point. First, the coefficient λ is not invariant for transitional flows; rather, it is sensitive to the spectrum of unstable frequencies. Thus, it is through the precise

$$\Lambda = -\frac{\rho_e}{\rho_w}\frac{\theta^2}{U_e}\left(\frac{\partial^2 u}{\partial y^2}\right)_w$$

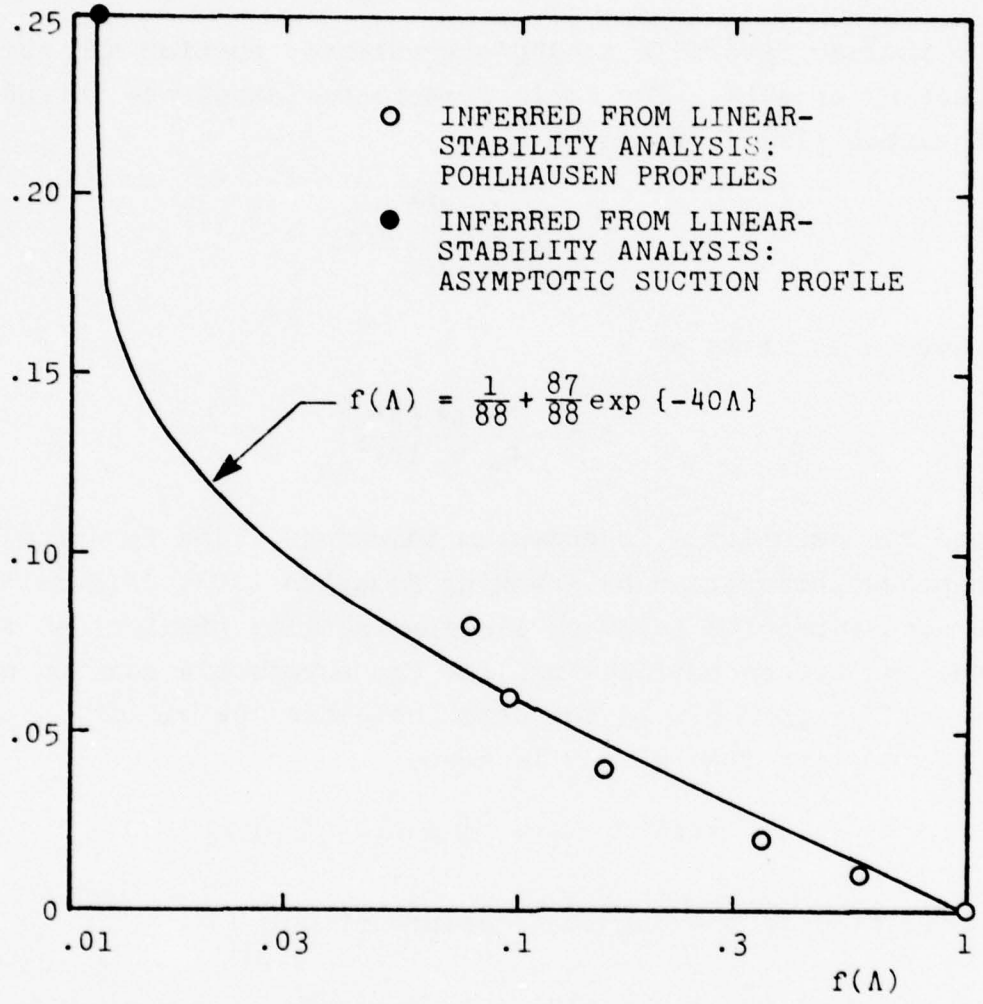

Figure 3. The stability function f(Λ).

value of λ that Tollmien-Schlichting waves implicitly appear in the model. Because the only transition-specific modifications to the model equations are for the coefficient λ [Equations (19)-(21)], it is hence unsurprising that ultimately we have chosen to rely upon linear-stability theory to set its value. Second, and of central importance to the present program, the coefficient λ also controls the rate at which disturbances are amplified beyond the critical point. The model's ability to accurately predict actual transition point location indicates that once the critical point is correctly established, the model provides an accurate simulation of the post-critical stages of transition with no further appeal to stability theory.

Given this insight, the whole concept of using turbulence-model equations to describe transition can be cast in a different light. On the one hand, time-averaging conceals many important physical aspects of transition mechanisms, particularly during the early linear-amplification phase. We are thus obligated to put some of the physics back into the equations which was lost through the time-averaging process; ergo, the modification to λ. On the other hand, assuming the latter phases of transition (i.e., close to the transition point) to be very rapid, the time-averaging process becomes a more plausible concept as the flow more nearly resembles a turbulent flow. (interestingly, the modification to λ has little effect on the latter stages of transition.) The turbulence-model transition-prediction approach thus has its strongest foundation in the latter stages of transition, precisely the regime where convnetional linear-stability methods are not well founded.

Thus, turbulence-model equations might most properly be viewed as a plausible alternative to the e^9 method. That is, a linear stability computation could be performed up to, and perhaps a bit beyond, the minimum-critical Reynolds number. Results

of the stability computation would define λ. Then, rather than continuing to solve eigenvalue problems to determine amplification factors up to the e^9 amplification point, the model equations could be used to predict transition location. As noted above, what we are currently doing is using a correlation of linear-stability minimum-critical Reynolds numbers to fix the value of λ.

Note that there is a fundamental premise underlying the notion that a computation with the model equations can replace the conventional e^9 procedure. The premise is that λ must be constant (or at least nearly constant) for varying Reynolds number and also be either constant or assume a universal variation through the boundary layer. If λ is either constant or assumes a universal variation through the layer, there is a rational procedure for setting its value in terms of the computed eigenfunctions. Likewise, if λ is nearly constant with Reynolds number, there may be a rational procedure for choosing an appropriate "average" value such as, for example, the value at the point where the linear-stability solution has been amplified to e^4 times its initial value. In other words, if linear-stability theory indicates that λ either (a) does not vary substantially with Reynolds number and with distance through the boundary layer or (b) varies in a universal manner, the closure approximation involving λ will be proven for very low Reynolds number.

2.2 THEORETICAL FORMULATION

As noted above, the overall objective of this research has been to synthesize linear-stability theory with the turbulence-model transition-prediction method. In the proposed synthesis, stability theory is used to locate the critical Reynolds number, R_c. Then, based on the stability solution at R_c (or perhaps at a slightly larger Reynolds number), initial conditions are established for a turbulence-model computation which proceeds from the point at which the stability solution is valid, up to

the transition point. To obtain a well-posed initial value problem for the turbulence-model computation, initial conditions are needed for three quantities, viz, e, ω and λ. In this subsection, these three quantities are specified in terms of linear-stability eigenfunctions.

Confining analysis to incompressible flows, Equations (13) and (14) provide an obvious way of defining e and ω profiles in terms of the stability theory eigenfunctions. To determine the initial value of λ we must examine the equation for e. For incompressible boundary layers, the equation for e simplifies to

$$u\frac{\partial e}{\partial x} + w\frac{\partial e}{\partial z} = \alpha^*\left|\frac{\partial u}{\partial y}\right| e - \beta^*\omega e + \frac{\partial}{\partial y}\left[(\nu + \sigma^*\varepsilon)\frac{\partial e}{\partial y}\right] \qquad (22)$$

where u and w are the mean velocity components in the streamwise, x, and lateral, z, directions. Note that in writing Equation (22) conventional boundary-layer approximations have been made and, in addition, the flow has been assumed parallel so that $v = 0$. The closure coefficient σ^* assumes a value of 1/2 while, in the limit of small Reynolds number based on turbulence intensity and scale [see Equation (10)], α^* simplifies to

$$\alpha^* = \frac{3}{10}\lambda$$

We now proceed to derive a relation between the closure coefficient λ and the stability solution. Noting the definition of e, we can derive an exact equation for its evolution by taking the v' moment of the v-momentum equation. The following equation, subject to the same approximations used in writing Equation (22), results for e.

$$u\frac{\partial e}{\partial x} + w\frac{\partial e}{\partial z} = -\frac{9}{2}\left\langle\frac{v'}{\rho}\frac{\partial p'}{\partial y}\right\rangle - \frac{9}{2}\nu\left\langle\left(\frac{\partial v'}{\partial y}\right)^2\right\rangle + \frac{\partial}{\partial y}\left[\nu\frac{\partial e}{\partial y} - \frac{9}{4}\langle v'^3\rangle\right] \qquad (23)$$

Comparison of Equations (22) and (23) shows that we have made the following two closure approximations:

$$\sigma^* \varepsilon \frac{\partial e}{\partial y} = - \frac{9}{4} \langle v'^3 \rangle \tag{24}$$

while

$$\left[\frac{3}{10} \lambda \left| \frac{\partial u}{\partial y} \right| - \beta^* \omega \right] e = - \frac{9}{2} \left\langle \frac{v'}{\rho} \frac{\partial p'}{\partial y} \right\rangle - \frac{9}{2} \nu \left\langle \left(\frac{\partial v'}{\partial y} \right)^2 \right\rangle \tag{25}$$

With some manipulation, the closure coefficients λ and σ^* can be expressed as follows.

$$\sigma^* = - \frac{4}{3\beta^*} \frac{\nu \langle v'^3 \rangle \langle (\partial v'/\partial y)^2 \rangle}{\langle v'^2 \rangle^2 \partial \langle v'^2 \rangle / \partial y} \tag{26}$$

$$\lambda = - \frac{10}{3} \frac{2 \left\langle \frac{v'}{\rho} \frac{\partial p'}{\partial y} \right\rangle - \nu \left\langle \left(\frac{\partial v'}{\partial y} \right)^2 \right\rangle}{\langle v'^2 \rangle \left| \partial u / \partial y \right|} \tag{27}$$

Equation (27) is the desired relation which can be used along with Equations (13) and (14) to define initial conditions for a turbulence-model computation. Potentially, Equation (26) provides a further check on the validity of the closure approximations. However, as will be shown below, Equation (26) predicts $\sigma^* = 0$ as a consequence of the assumed linearity of the solution.

In the linear-stability solution, the velocity and pressure fluctuations v' and p' are written as

$$v'(x,y,z,t) = U_\infty \phi(y) \exp[i(\hat{\alpha}x + \hat{\beta}z - \hat{\omega}t)] \tag{28}$$

$$p'(x,y,z,t) = \rho U_\infty^2 \pi(y) \exp[i(\hat{\alpha}x + \hat{\beta}z - \hat{\omega}t)] \tag{29}$$

where t denotes time, U_∞ is freestream velocity, $\hat{\alpha}$ and $\hat{\beta}$ are wave numbers, $\hat{\omega}$ is frequency, and the functions $\phi(y)$ and $\pi(y)$ are the complex amplitude functions of the disturbance flow variables v' and p'.

To evaluate the time-averaged quantities appearing in Equations (13), (14), (26) and (27) we use the following definition:

$$\langle\psi\rangle = \lim_{\hat{\omega}T\to\infty} \frac{1}{2T} \int_{t-T}^{t+T} \psi(x,y,z,t')dt' \tag{30}$$

An immediate consequence of the assumed linearity of the solution is that correlations of odd order vanish, e.g.,

$$\langle v'\rangle = \langle v'^3\rangle = \langle v'^5\rangle = \ldots = 0 \tag{31}$$

Thus, as noted above, Equation (26) implies that $\sigma^* = 0$. Although σ^* is postulated to be 1/2 by Wilcox and Traci, this discrepancy is of little consequence as the diffusion terms in the e equation play an insignificant role in transitional flows.

Working with the real parts of the linear-stability solution functions, performing all time-averages indicated in Equations (13), (14) and (27), and denoting local Reynolds number by R yields the following:

$$e/U_\infty^2 = \frac{9}{8} (\phi_r^2 + \phi_i^2) \tag{32}$$

$$\frac{\nu\omega}{U_\infty^2} = \frac{3}{\beta^* R^2} \frac{(d\phi_r/dy)^2 + (d\phi_i/dy)^2}{(\phi_r^2 + \phi_i^2)} \tag{33}$$

$$\lambda = -\frac{10}{3}\,\frac{2(\phi_r d\pi_r/dy + \phi_i d\pi_i/dy) - R^{-1}\left[(d\phi_r/dy)^2 + (d\phi_i/dy)^2\right]}{(\phi_r^2 + \phi_i^2)\,|\partial U/\partial y|} \qquad (34)$$

where y is now dimensionless distance from the surface, $U = \bar{u}/U_\infty$, and subscripts r and i denote real and imaginary part. Equations (32) - (34) are the desired relations which can be used to define initial conditions for a turbulence-model computation in terms of a given linear-stability solution.

2.3 EVALUATION OF THE CLOSURE COEFFICIENT λ

Having derived Equations (32)-(34) above, the next step is to perform a linear-stability computation and to examine the resultant profiles, particularly the λ profile. The most sensible starting point is to begin with the Blasius boundary layer. A large number of stability computations have been performed with the Mack[17] stability program; all computations have been done with the spatial amplification theory option. Both Reynolds number and frequency have been varied in order to determine the variation of λ throughout the Reynolds-number/frequency plane.

Prior to examining results of the computations, it is instructive to recall that the basic premise of forming a synthesis of linear stability and turbulence-model methods is that two conditions be satisfied. The first condition is that the closure coefficient λ be either relatively weak function of distance through the boundary layer or, at least, assume a similar variation for all unstable frequencies; this condition validates the closure approximation defined in Equation (25). The second condition is that λ vary slowly with Reynolds number; this condition is needed (a) to validate Equation (25) and (b) to eliminate solution sensitivity to initial conditions. Note also that we hope to find the average value of λ to be reasonably close to the postulated Blasius value, viz, $\lambda = 1/11$.

Figure 4 shows computed λ profiles at nine Reynolds numbers corresponding to one stable case, one neutrally stable case, and seven unstable cases corresponding to amplification from the neutral case by factors of e^n with values of n ranging from 0 to 10; for all nine cases the frequency is given by

$$Fr = \hat{\omega}\nu/U_\infty^2 = 2\cdot 10^{-5} \tag{35}$$

We are thus following the evolution of λ for a constant-frequency disturbance initiated at a Reynolds number upstream of the neutral point corresponding to the frequency given in Equation (35).

As shown, although λ varies rapidly with y near the surface, all nine curves display approximately the same variation. However, above a vlaue of $\eta = y\sqrt{U_\infty/\nu x}$ of about 2, the various λ profiles vary rapidly with η and do so in dissimilar manner for amplification ratios up to $e^{4.56}$. For example, at the lowest Reynolds number (for which the solution is stable), λ is negative above $\eta \doteq 2$. As we move to the neutral point we find that λ vanishes for values of η in excess of 2.5. Then as Reynolds number increases, λ varies more and more rapidly with η and asymptotes to a single curve for amplification ratios in excess of between e^3 and e^4.

Figure 5 shows similar curves for a dimensionless frequency Fr given by

$$Fr = 3\cdot 10^{-5} \tag{36}$$

Again, the curves collapse to a single curve for amplification ratios in excess of e^4.

Computations have been performed for frequencies covering the entire stability diagram. For each frequency considered, the computed λ profiles always asymptote to a universal profile beyond the e^4 point with a subtle qualification. That is, referring to Figure 6, as Reynolds number increases, the upper branch of the stability diagram eventually is reached and we

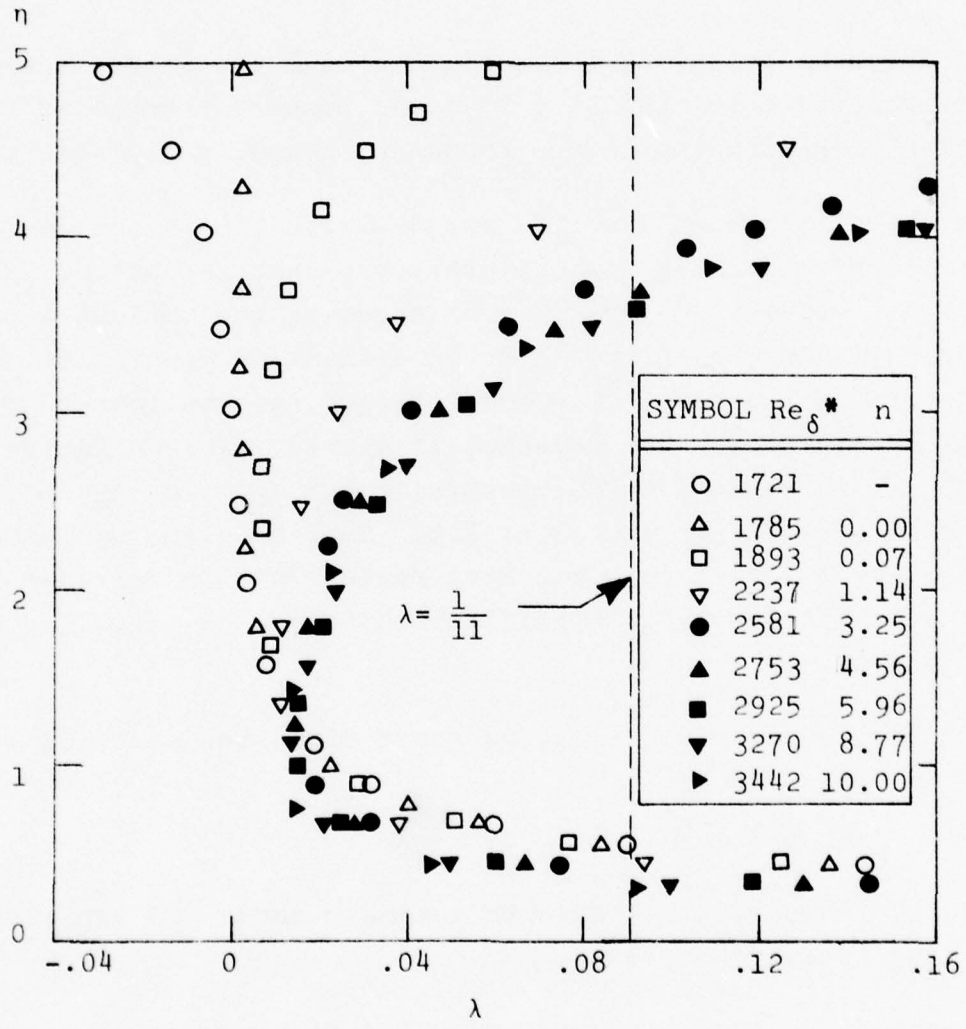

Figure 4. Computed λ profiles for dimensionless frequency Fr = $2 \cdot 10^{-5}$.

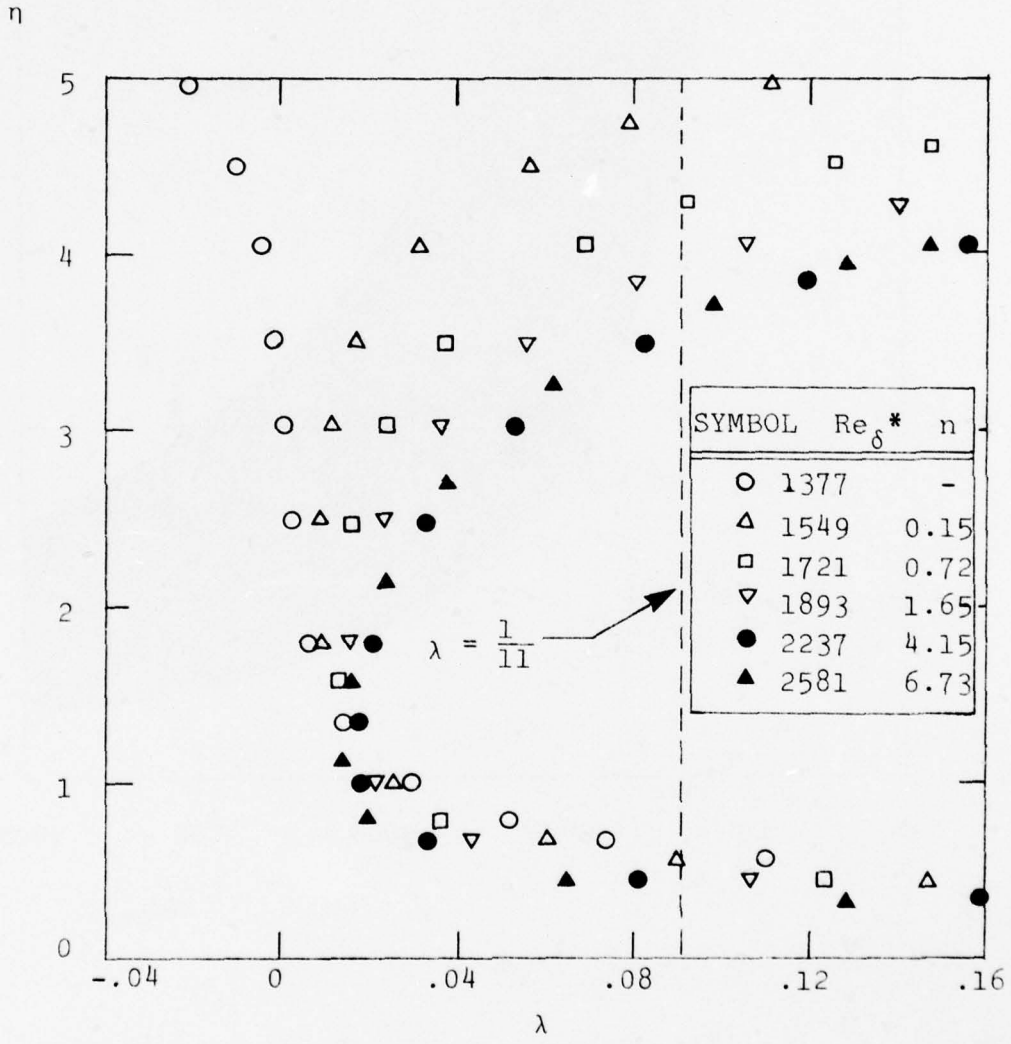

Figure 5. Computed λ profiles for dimensionless frequency Fr = $3 \cdot 10^{-5}$.

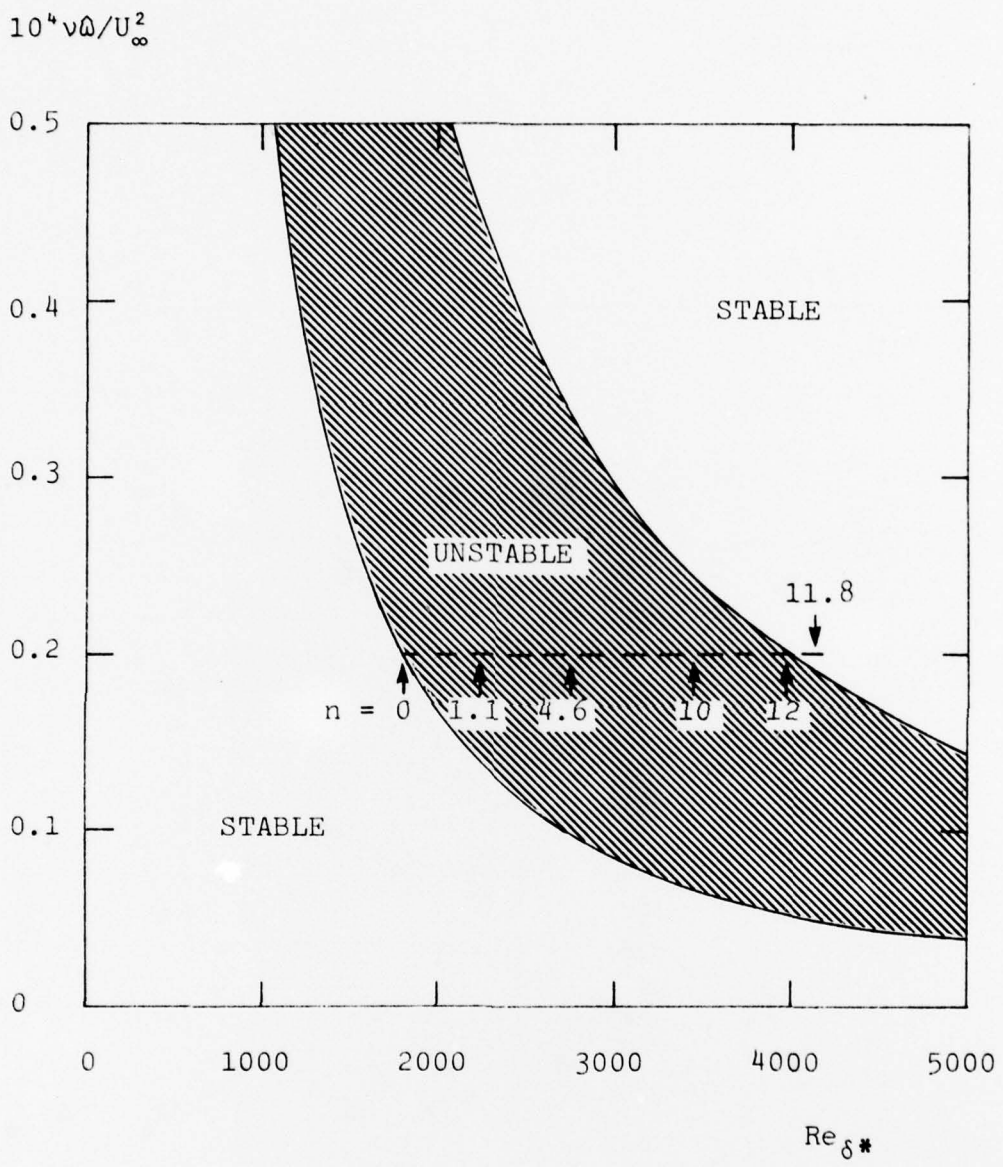

Figure 6. Stability diagram for the Blasius boundary layer depicting a constant frequency trajectory; n denotes solution amplification of e^n.

again enter a stable region. As we approach this upper neutral point, the λ profiles begin to fall back to those typical of low Reynolds numbers.

The rapid variation of λ near $\eta=0$ results from a breakdown in the basic closure approximations near the surface. That is, the production term in the $\langle v'^2 \rangle$ equation, $\langle -\frac{v'}{\rho} \frac{\partial p'}{\partial y} \rangle$, goes to zero quadratically with distance from the surface so that, in terms of η,

$$\langle -\frac{v'}{\rho} \frac{\partial p'}{\partial y} \rangle \sim \eta^2 \qquad \text{as} \qquad \eta \to 0 \qquad (37)$$

By contrast, the modeled production term for $Re_T \to 0$ behaves as

$$\frac{3}{10} \lambda \frac{\partial u}{\partial y} e \sim \lambda \eta^4 \qquad \text{as} \qquad \eta \to 0 \qquad (38)$$

Consequently, close to the surface we ultimately have

$$\lambda \sim \eta^{-2} \qquad \text{as} \qquad \eta \to 0 \qquad (39)$$

This modeling shortcoming is of little consequence as dissipation exceeds production near $\eta=0$. Consequently, for the remainder of this discussion our focus will be upon the region between $\eta=1$ and the outer edge of the boundary layer, $\eta=5$.

Figure 7 shows computed λ profiles for several frequencies and amplification ratios. As shown, all of the computed λ profiles cluster about the approximate profile defined by

$$\lambda = .0093 + .0015 \exp\left[-\frac{10}{7}(\eta-1)\right] \qquad (40)$$

Hence, one of the basic requirements for establishing a turbulence-model/linear-stability synthesis appears to be satisfied, viz, the λ profile appears to approach a universal (i.e., independent of frequency) limiting profile as amplification ratio increases.

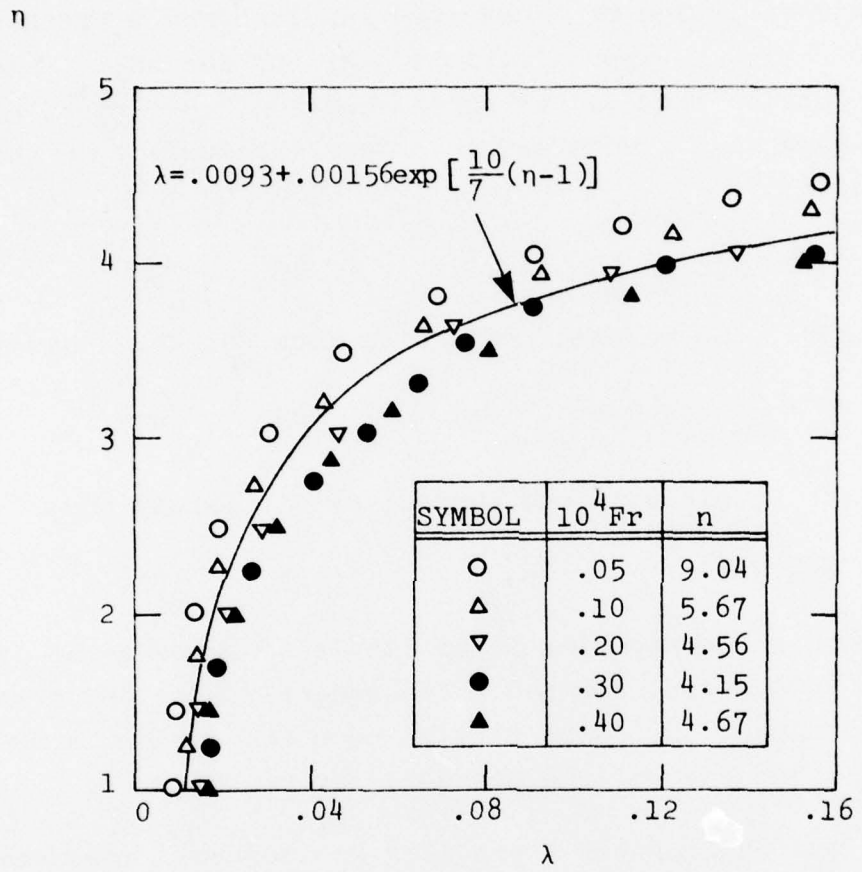

Figure 7. Profiles of the closure coefficient λ for various frequencies and amplification ratios.

To determine the rate of approach to the asymptotic profile, it is convenient to examine the average value of λ defined as follows.

$$\bar{\lambda} \equiv \frac{1}{4} \int_1^5 \lambda \, d\eta \tag{41}$$

Figure 8 shows $\bar{\lambda}$ as a function of displacement thickness Reynolds number, $Re_\delta{}^*$; note that $Re_{\delta_i}{}^*$ denotes the neutral-stability value of $Re_\delta{}^*$ for a given frequency. As shown, for the higher frequencies $\bar{\lambda}$ approaches its asymptotic value most rapidly. For $Fr = 0.5 \cdot 10^{-5}$, the lowest frequency at which computations have been done, the approach to the asymptotic value is the least rapid. A key feature of all the curves is that their asymptotic values lie between $\bar{\lambda} = .066$ and $\bar{\lambda} = .083$, as compared to the postulated turbulence-model value of .091.

Further examination of the $\bar{\lambda}$ variation with Reynolds number shows that for the higher frequencies, the peak value is achieved at an amplification ratio of about e^4 while, for the lowest frequency, $\bar{\lambda}$ is about half its asymptotic value at this ratio. Figure 9 presents the variation of $\bar{\lambda}$ with frequency for amplification ratio e^4, including a correlation of the computed values; the correlation is:

$$\bar{\lambda}_{n=4} = \frac{7}{55} \left\{ 1 - \exp \left[-\frac{25}{3} (10^4 Fr) \right] \right\} \tag{42}$$

The asymptotic values of $\bar{\lambda}$ are also shown for reference. Two key conclusions can be drawn from the observed variation of $\bar{\lambda}$. First, beyond an amplification ratio of e^4, $\bar{\lambda}$ varies slowly with Reynolds number. Second, $\bar{\lambda}$ is only weakly frequency dependent for frequencies in excess of $Fr = 1.0 \cdot 10^{-5}$. These two points lend further credence to the second of the two basic hypotheses underlying a synthesis of turbulence-model and linear-stability theories.

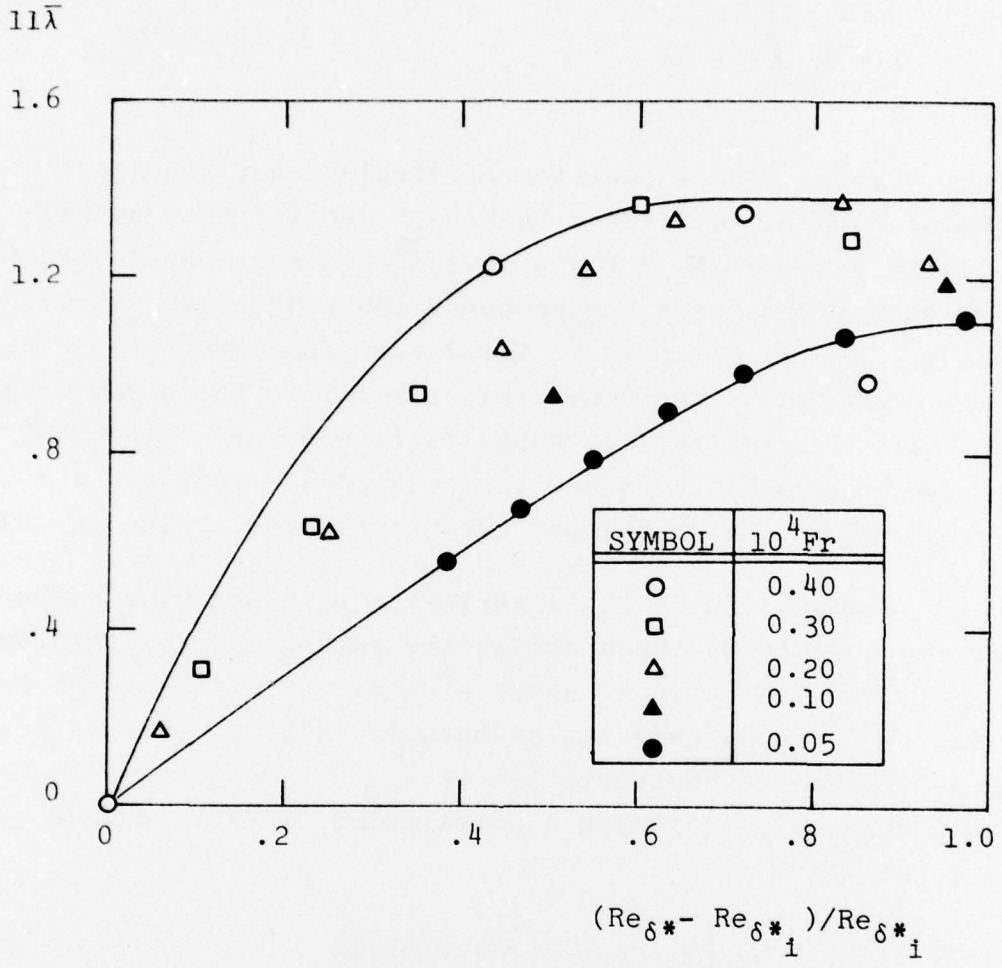

Figure 8. Variation of $\bar{\lambda}$ with Reynolds number for several frequencies.

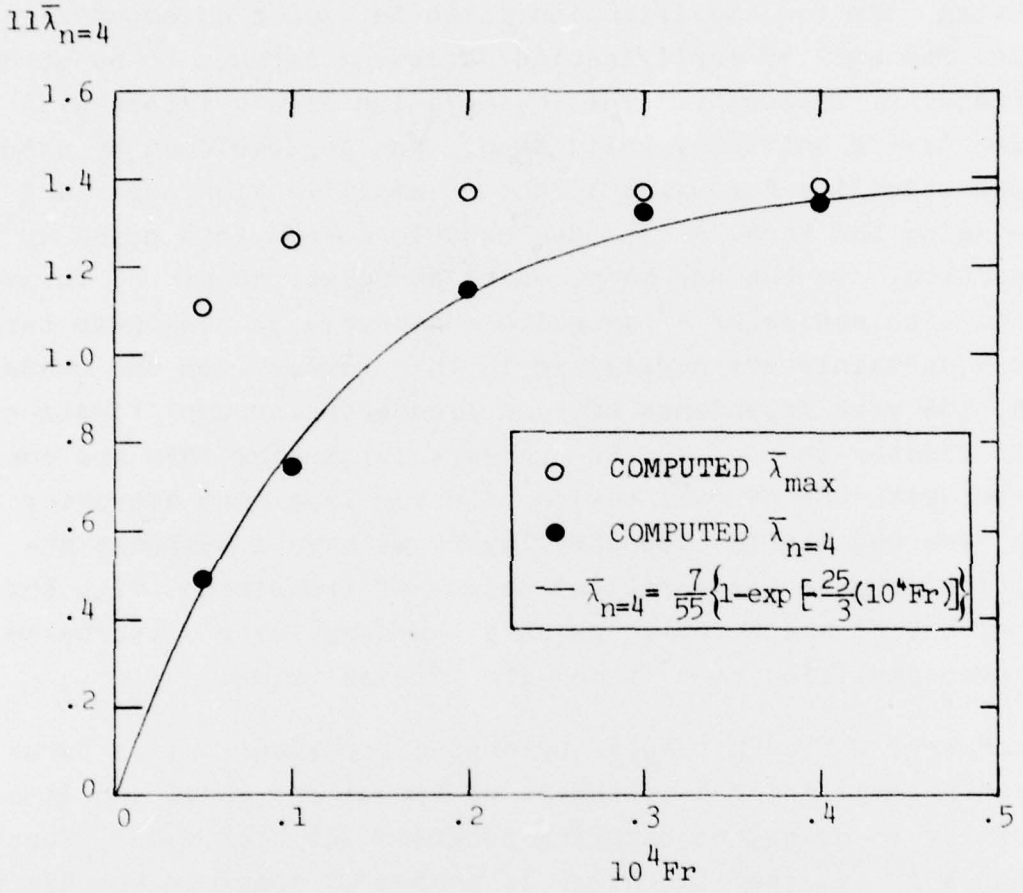

Figure 9. Correlation of the average value of λ with frequency for an amplification ratio of e^4.

3. DISCUSSION

Results presented in Section 2.3 show that for the Blasius boundary layer the closure coefficient λ approaches a universal limiting form for amplification ratio in excess of about e^4 while, for smaller amplification ratios, λ appears to be strongly frequency dependent. This observation is consistent with the notion that a uniformly valid theory can be developed by using linear stability theory up to the e^4 amplification point and by then using the turbulence-model equations from this point up to transition. On the one hand, using stability theory up to amplification ratios of e^4 is quite reasonable as nonlinear terms almost certainly are negligible in this regime. On the other hand, the weak dependence of λ on frequency for amplification ratio greater than e^4 and the universal limiting form are consistent with the overall notion of using long-term averaging. Thus, for the Blasius boundary layer, we have a suitable definition for the post-critical stages of transition, viz, the stages beyond the point at which a boundary-layer disturbance has been amplified to e^4 times its initial value.

In summary, although results presented represent only a first cut at accomplishing a synthesis of turbulence-model and linear-stability theories, encouraging progress has been made. Further research in two specific areas is needed to complete the synthesis. The first area needing further investigation is evaluation of λ for boundary layers with pressure gradient, suction and surface heat transfer. In so doing, we can determine whether a profile such as that defined in Equation (40) applies to all boundary layers or if straightforward generalizations can be made to devise a universally applicable λ profile. The second area is use of Equation (40) in a turbulence-model computation to determine solution sensitivity to (a) the point of initiation (e.g., e^4 amplification point) and (b) freestream turbulence.

Results of this study suggest that when this research has been done our ultimate goal of establishing a physically sound alternative to the empirical Smith-van Ingen e^9 procedure can be realized.

REFERENCES

1. Wazzan, A.R. and Smith, A.M.O., "Laminarization of Water Boundary Layers over Bodies of Revolution," Paper presented at RAND Low-Speed Boundary-Layer Transition Workshop, The RAND Corp, Santa Monica, CA (Sept 13-15, 1976).

2. Smith, A.M.O. and Gamberoni, N., "Transition, Pressure Gradient, and Stability Theory," Report ES 26388, Douglas Aircraft Co, Inc, El Segundo, CA (1956).

3. Van Ingen, J.L., "A Suggested Semi-empirical Method for the Calculation of the Boundary Layer Transition Region," Dept Aero Eng, Inst of Technology, Delft, Report V.T.H. 74 (1956).

4. Wilcox, D.C., "Turbulence-Model Transition Predictions," AIAA Journal, Vol 13, No 2, pp 241-243 (1975).

5. Jones, W.P. and Launder, B.E., "Calculation of Low Reynolds Number Phenomena with a Two-Equation Model of Turbulence," Int J Heat and Mass Trans, Vol 16, pp 1119-1129 (1973).

6. Donaldson, C. duP., "A Computer Study of an Analytical Model of Boundary Layer Transition," AIAA Paper 68-38 (1968).

7. Wilcox, D.C. and Chambers, T.L., "Numerical Simulation of Nosetip Transition: Model Refinement and Validation," AFOSR-TR-76-1112 (July 1976).

8. Chambers, T.L. and Wilcox, D.C., "Application of the Turbulence-Model Transition-Prediction Method to Flight-Test Vehicles," Turbulence in Internal Flows, pp 233-247, S.B. Murthy Ed, Hemisphere Pub Co (1976).

9. Wilcox, D.C. and Chambers, T.L., "Transition Simulation for Incompressible Boundary Layers and Heated Hydrodynamic Bodies," DCW Industries Report DCW-R-10-01 (July 1976).

10. Wilcox, D.C. and Traci, R.M., "A Complete Model of Turbulence," AIAA Paper 76-351, San Diego, CA (July 1976).

11. Wilcox, D.C., "A Model for Transitional Flows," AIAA Paper 77-125, Los Angeles CA (Jan 1977).

12. Laufer, J., "The Structure of Turbulence in Fully Developed Pipe Flow," NACA 1174 (1952).

13. Wilcox, D.C., "Calculation of Turbulent Boundary-Layer Shock-Wave Interaction," AIAA Journal, Vol 11, No 11, pp 1592-1594 (1973).

14. Wilcox, D.C., "Numerical Study of Separated Turbulent Flows," AIAA Paper 74-584 (1974).

15. Wilcox, D.C. and Chambers, T.L., "Streamline Curvature Effects on Turbulent Boundary Layers," AIAA Journal, Vol 15, No 4, pp 574-580 (Apr 1977).

16. Schlichting, H., Boundary Layer Theory, Fourth Ed, McGraw-Hill, p 414 (1960).

17. Mack, L.M., "Transition and Laminar Instability," JPL Publication 77-15 (May 1977).

LIST OF SYMBOLS

SYMBOL	DEFINITION
e	Turbulent mixing energy defined in Equation (13)
$f(\Lambda)$	Empirical stability function
Fr	Dimensionless frequency, $\nu\hat{\omega}/U_\infty^2$
h	Static enthalpy
$H(\Lambda)$	Heaviside stepfunction
k	Roughness height
n	Amplification ratio exponent, e^n
p	Static pressure
Pr_L, Pr_T	Laminar, turbulent Prandtl numbers
q_j	Heat flux vector
R	Plate-length Reynolds number
Re_T	Turbulent Reynolds number defined in Equation (11)
$Re_{\tilde{x}}$	Neutral-stability Reynolds number
Re_{x_c}	Minimum-critical Reynolds number
Re_{δ^*}	Displacement-thickness Reynolds number
S_{ij}	Mean strain rate tensor
T'	Freestream turbulence intensity
u,v,w	Velocity components in x,y,z directions
u_j	Velocity vector
u_τ	Friction velocity
U_∞	Freestream velocity
x,y,z	Cartesian coordinates in streamwise, normal, lateral directions
x_j	Position vector
α,α^*	Closure coefficients
$\hat{\alpha}$	Complex wave number
β,β^*	Closure coefficients
$\hat{\beta}$	Complex wave number
δ^*	Displacement thickness
ε	Kinematic Eddy viscosity

LIST OF SYMBOLS

SYMBOL	DEFINITION
η	Blasius similarity variable
θ	Momentum thickness
λ	Closure coefficient
$\overline{\lambda}$	Average value of λ defined in Equation (41)
$\overline{\lambda}_{max}$	Peak value of $\overline{\lambda}$
$\overline{\lambda}_{n=4}$	Value of $\overline{\lambda}$ when amplification ratio is e^4
Λ	Modified Pohlhausen parameter
μ	Molecular viscosity
ν	Kinematic molecular viscosity
$\pi(y)$	Complex pressure eigenfunction
ρ	Density
σ, σ^*	Closure coefficients
τ_{ij}	Stress tensor
$\phi(y)$	Complex normal-velocity eigenfunction
ω	Turbulent dissipation rate defined in Equation (14)
$\hat{\omega}$	Frequency
ℓ	Turbulent length scale, $e^{1/2}/\omega$

Subscripts and Superscripts

e	Boundary layer edge value
i	Imaginary part
r	Real part
w	Surface or wall value

Other Notation

For a given variable ψ:

$\langle\psi\rangle, \overline{\psi}$	Long-time-averaged value of ψ defined in Equation (30)
ψ'	Fluctuating part of ψ

DISTRIBUTION LIST

Chief of Naval Research
Department of the Navy
Arlington, VA 22217
ATTN: Vehicle Technology Program
Code 211 5
Code 222 1
Code 438 1

Chief of Naval Development
Department of the Navy
Washington, DC 20360
ATTN: NAVMAT 0331 1

Naval Sea Systems Command
Code 09GS (Library)
Washington, DC 20362 1

Naval Sea Systems Command
Code 03512
Washington, DC 20362
ATTN: Dr. T. Pierce 1

David Taylor Naval Ship Research
& Development Center
Bethesda, MD 20034
ATTN: Code 16 1
Code 19 1
Code 154 1

Naval Research Laboratory
Washington, DC 20375
ATTN: Technical Information
Office, Code 2627 1
Library, Code 2629 1

Superintendent
U. S. Naval Academy
Annapolis, MD 21402 1

Superintendent
U. S. Naval Postgraduate School
Monterey, CA 93940 1

Director
Office of Naval Research Branch Office
495 Summer Street
Boston, MA 02210 1

Director
Office of Naval Research Branch Office
536 South Clark Street
Chicago, IL 60605 1

Director
Office of Naval Research Branch Office
1030 E. Green Street
Pasadena, CA 91106 1

Technical Library
Naval Coastal Systems Laboratory
Panama City, FL 32401 1

Defense Documentation Center
Cameron Station
Alexandria, VA 22314 12

Naval Underwater Systems Center
Code SB 323
Newport, RI 02840 1

Air Force Office of Scientific Research
Bldg. 410
Bolling AFB, DC 20332
ATTN: Aerospace Sciences (NA) 1

Army Research Office
P. O. Box 12211
Research Triangle Park, NC 27709
ATTN: Dr. R. Singleton 1

National Aeronautics and Space
Administration
600 Independence Avenue, SW
Washington, DC 20546
ATTN: Code RAA 1
Code RAV 1

National Aeronautics and Space Administration
Langley Research Center
Hampton, VA 23665
ATTN: Dr. D. Bushnell 1

Lockheed Missiles & Space Co., Inc.
Huntsville Research & Engineering Ctr.
P. O. Box 1103
Huntsville, AL 35807
ATTN: Mr. A. Zalay 1

General Dynamics/Convair Div.
Kearny Mesa Plant
P. O. Box 80847
San Diego, CA 92138
ATTN: Dr. E. Levinsky 1

Flow Research Company
P. O. Box 5040
Kent, WA 98031
ATTN: Dr. E. Murmann 1

Dynamics Technology, Inc.
3838 Carson Street
Suite 110
Torrance, CA 90503
ATTN: Dr. Denny Ko 1

Advanced Technology Center, Inc.
P. O. Box 6144
Dallas, TX 75222
ATTN: Dr. C. Haight 1

Massachusetts Institute of Technology
Department of Ocean Engineering
Cambridge, MA 02139
ATTN: Prof. P. Leehey 1

Massachusetts Institute of Technology
Department of Aeronautics and Astronautics
Cambridge, MA 02139
ATTN: Prof. M. Landahl 1

California Institute of Technology
Graduate Aeronautical Laboratories
California Institute of Technology
Pasadena, CA 91125
ATTN: Prof. H. W. Liepmann 1

Rand Corporation
1700 Main Street
Santa Monica, CA 90406
ATTN: Dr. W. S. King 1

Case Western Reserve University
Dept. of Fluid, Thermal and Aerospace Sciences
Cleveland, OH 44106
ATTN: Prof. E. Reshotko 1

Illinois Institue of Technology
Dept. of Mechanics and Mechanical and Aerospace Engineering
3300 South Federal Street
Chicago, IL 60616
ATTN: Dr. Mark V. Morkovin 1

University of Southern California
Dept. of Aerospace Engineering
University Park
Los Angeles, CA 90007
ATTN: Prof. John Laufer 1

Virginia Polytechnic Institute and State University
Dept. of Engineering Science and Mechanics
Blacksburg, VA 24061
ATTN: Professor A. H. Nayfeh 1

California State University, Long Beach
Dept. of Mechanical Engineering
Long Beach, CA 90840
ATTN: Professor T. Cebeci 1

Cambridge Hydrodynamics Laboratory
54 Baskin Road
Lexington, MA 02173
ATTN: Dr. S. A. Orszag 1

Jet Propulsion Laboratory
4800 Oak Grove Drive
Pasadena, CA 91103
ATTN: Mr. Leslie M. Mack 1